CMS Physics Analysis Summary

Contact: cms-pag-conveners-fsq@cern.ch 2014/11/12

Measurement of the underlying event activity using charged particle jets in proton-proton collisions at $\sqrt{s}$ = 2.76 TeV

The CMS Collaboration

Abstract

A measurement of the underlying event (UE) activity in proton-proton collisions is performed using events with a leading charged particle jet produced at central pseudorapidity ($|\eta^{\text{jet}}| < 2$) and of transverse momentum in the range of 1 to 100 GeV. The analysis uses 0.3 nb^{-1} of integrated luminosity at the centre-of-mass energy of 2.76 TeV at the LHC by the CMS experiment. The UE activity is measured as a function of p_T^{jet} in terms of the average multiplicity and scalar-p_T sum of charged particles with $|\eta| < 2$ and $p_T > 0.5$ GeV in the azimuthal region *transverse* to the leading jet direction. By dividing the *transverse* region into the minimum and maximum activity sides with respect to the leading jet, further information on the dynamics of the UE is obtained. The measurements are compared to previous results at 0.9 and 7 TeV and to predictions of several QCD-inspired models providing constraints of the parameters involved.

1 Introduction

The underlying event (UE) activity in hard hadron-hadron interactions is all the additional activity of the hadrons on top of the hard parton scattering. The UE consists in initial- and final-state radiation (ISR, FSR) from the hard process partons, but also from softer secondary partonic scatters in the same collision (multiple parton interactions, or MPI), the hadronisation of emerging hard partons as well as quantum chromodynamics (QCD) colour connections between partons and the beam remnants or even soft rescattering of the beam remnants. An accurate understanding of the UE, with a proper modeling of its main component coming from MPI, is then required to perform searches for new physics and precise measurements of standard model processes at high energies as it cannot be unambiguously separated from the hard scattering process and hence modify important observables. The semihard and low-momentum QCD processes, which dominate the UE cannot be described completely with perturbative QCD methods and require a phenomenological description containing parameters, which must be tuned to the data.

The topological structure of hard hadron-hadron interactions can be used to define experimental observables which are very sensitive to the UE, like the study of particle properties in regions away from the direction of the emerging products of the hard scattering. At the Tevatron, the CDF experiment measured UE observables with inclusive jet and Drell–Yan events in $p\bar{p}$ collisions at centre-of-mass energy ($\sqrt{s}$) of 0.63, 1.8 and 1.96 TeV [1–3]. In pp collisions at the LHC, the CMS, ATLAS and ALICE experiments have carried out UE measurements at $\sqrt{s} = 0.9$ and 7 TeV using events containing a leading jet [4, 5], a leading charged particle [6, 7], or a Z boson [8]. In this paper, we study the UE activity by measuring the average multiplicity and scalar transverse momentum sum (Σp_T) densities of charged particles in the azimuthal *transverse* region with respect to the leading charged particle jet in pp collisions at $\sqrt{s} = 2.76$ TeV.

At a given centre-of-mass energy, the UE activity is expected to increase with the hard scale of the interaction. Indeed on average the impact parameter is decreasing with increasing hard scale, a feature which in turn enhances MPI until it starts to saturate [9, 10]. At the same time, the activity related to the ISR and FSR components continues to increase with the hard scale. For events with the same hard scale, the MPI activity is expected to increase with $\sqrt{s}$ [9, 10]. Hence studying the UE as a function of the hard scale at several centre-of-mass energies provides an insight into the UE dynamics, its evolution with the collision energy, and further constrains the model parameters.

This analysis summary is organised as follows: in section 2 we describe the main features of the Monte Carlo event generators used in this study, which are relevant to the description and prediction of UE properties. Section 3 briefly describes the experimental methods, observables, event and track selection as well as a discussion on corrections and systematic uncertainties of this measurement. In section 4, the results are presented and in section 5, the summary.

2 Monte Carlo models

In this analysis, PYTHIA6 [11], PYTHIA8 [12] and HERWIG++ [13] generators are used, with various tunes that are described below.

The $2 \to 2$ non-diffractive processes, including multiple partonic interactions (MPI), are described by lowest-order perturbative QCD with the divergence of the cross-section as $p_T \to 0$ regulated with a phenomenological model. There are many tunable parameters that control,

among other things, the behaviour of this regularisation, the matter distribution of partons within the hadrons, and colour reconnection. When p_T-ordered parton showers are used, the MPI and parton shower are interleaved in one common sequence of decreasing p_T values. For PYTHIA6 the interleaving is between the initial-state shower and MPI only, while for PYTHIA8 it also includes final-state showers. Since the p_T-ordered showers and interleaving with MPI [14] are considered to be a model improvement [11], the most recent PYTHIA6 tunes are made with this configuration. This is also the only configuration available in PYTHIA8.

HERWIG++ is another general purpose generator, but with a different approach: it uses an angular-ordered parton shower and the cluster hadronisation model [13]. It has an MPI model similar to the one used by the PYTHIA generators, with tunable parameters for regularising the behaviour at very low momentum transfer, but does not include the interleaving with the parton showers. Inclusive hadron-hadron collisions are simulated by applying the MPI model to events with no hard scattering. It is therefore possible to generate an event with zero $2\rightarrow2$ partonic scatters, in which only beam remnants are produced, with nothing in between them. While HERWIG++ has no explicit model for diffractive processes, these zero-scatter events will look similar to double-diffractive dissociation.

The introduction of MPI models (extending the perturbative description in a soft regime) in Monte Carlo tools, improved the description of past observations related to the final-state multiplicity of particle production. Only a phenomenological approach can be used, due to the fact that its dynamics are not well understood since they are governed by soft and semi-hard interactions. In almost all cases, MPI are implemented by assuming a Poissonian distribution of elementary partonic interactions, with an average number depending on the impact parameter of the hadronic collision [9, 10]. The cross section is characterised by a stronger dependence on the incoming parton flux (as compared with the single pair case). Therefore MPI becomes increasingly important at higher centre-of-mass energies [9, 10] of the colliding hadrons, where partons with smaller and smaller fractional momenta play an active role. The dependence of the UE activity on the energy scale is well described by Monte Carlo [4–8], illustrating the universality of MPIs in different topologies and production processes. This universality is also indicated by the similarity between the UE activity in DY [8] and hadronic events [4–7], although these events have different types of radiation. In PYTHIA6, PYTHIA8 and HERWIG++, the energy dependence of MPI is modelled as an exponential function of the centre-of-mass energy with tunable parameters [11–13]. HERWIG++ also assumes that MPI varies with the colliding energy and has recently automated this process.

In this analysis, several event generators tunes are used for comparison with the data. These are the PYTHIA6 version 6.426 [11] tune Z2* [15] and tune CUETP6S1 [16], PYTHIA8 version 8.175 [12] tune 4C [17] and CUETP8S1 [16], and HERWIG++ 2.7 tune UE-EE-5C [13, 18]. These event generators and tunes differ in the treatment of initial- and final-state radiation, hadronisation, colour reconnections, and cutoff values for the MPI mechanism. These tunes were obtained from comparisons between predictions and data aimed at providing a reasonable description of existing UE data, especially those measured with LHC pp collision. However, minimum bias observables and data from the Tevatron, collected at lower centre-of-mass energies, were also used to obtain some of these tunes.

3 Experimental methods

The central feature of the CMS apparatus is a superconducting solenoid of 6 m internal diameter, providing a magnetic field of 3.8 T. Within the superconducting solenoid volume there are several complementary detectors: a silicon pixel and strip tracker, a lead tungstate crys-

tal electromagnetic calorimeter (ECAL), and a brass/scintillator hadron calorimeter (HCAL), each composed of a barrel and two endcap sections. The silicon tracker measures charged particles within the pseudorapidity range $|\eta| < 2.5$. For non-isolated particles of $1 < p_{\mathrm{T}} < 10$ GeV and $|\eta| < 1.4$, the track resolutions are typically 1.5% in p_{T} and 25–90 (45–150) μm in the transverse (longitudinal) impact parameter [19]. Two of the CMS subdetectors acting as LHC beam monitors, the Beam Scintillation Counters (BSC) and the Beam Pick-up Timing for the eXperiments (BPTX) devices, were used to trigger the detector readout. The BSC are located along the beam line on each side of the IP at a distance of 10.86 m and are sensitive in the range $3.23 < |\eta| < 4.65$. The two BPTX devices, which are located inside the beam pipe at distances of 175 m from the IP, are designed to provide precise information on the bunch structure and timing of the incoming beams, with a time resolution better than 0.2 ns. A more detailed description of the CMS detector, together with a definition of the coordinate system used and the relevant kinematic variables, can be found in Ref. [20].

3.1 Observables

In this analysis we follow the same methodology as in the previous CMS analysis [4]. Charged particle jets and charged particles produced at central pseudorapidity ($|\eta| < 2$) with transverse momentum larger than 1 GeV and 0.5 GeV, respectively, are used to study the UE properties. The direction of the leading charged particle jet in the event is used to select charged particle in its azimuthal *transverse* region defined by $60^\circ < |\Delta\phi| < 120^\circ$, where $\Delta\phi$ is the relative azimuthal distance between a charged particle and the leading jet. The UE is measured in terms of particle and Σp_T densities as a function of the leading jet transverse momentum p_T^{jet} defined as the hard scale of the interaction. The particle ($\langle N_{ch} \rangle$ / $[\Delta\eta\Delta(\Delta\phi)]$) and Σp_T ($\langle \sum p_T \rangle$ / $[\Delta\eta\Delta(\Delta\phi)]$) densities are computed, respectively, as the average number of primary charged particles and the average of the scalar sum of their transverse momenta per unit of η and per unit of $\Delta\phi$.

As suggested in [21], the *transverse* region can be studied in more details by separating the $60^\circ < \Delta\phi < 120^\circ$ and the $-120^\circ < \Delta\phi < -60^\circ$ regions and identifying the region with higher and lower activity, separately for the particle multiplicity and the p_T sum, as *transMAX* and *transMIN* respectively. The difference between *transMAX* activity and *transMIN* activity is used to construct the *transDIF* activity. The resulting particle and Σp_T densities are expected to be sensitive to different components of the UE activity.

For events with large initial- and final-state radiation, the *transMAX* region contains the third jet while both *transMAX* and *transMIN* regions receive contributions from the MPI and beam-beam remnants. The *transMIN* activity is therefore sensitive to MPI and beam-beam remnants and the *transDIF* activity (*transMAX* minus *transMIN*) is sensitive to initial- and final-state radiation.

3.2 Event and track selection

The present analysis is performed with a data sample of proton-proton collisions collected by the CMS detector at $\sqrt{s} = 2.76$ TeV during a dedicated run of few days in March 2011, corresponding to an integrated luminosity of 0.3 nb^{-1} and a pile-up of 6.2% (average of 0.12 collisions per bunch crossing). Very similar selection conditions as the previous CMS analysis of the UE activity with leading charged jet at 0.9 and 7 TeV [4] are applied. Minimum bias events were recorded by requesting activity in both BSC counters in coincidence with signals from both BPTX devices. To enhance the event sample and reduce statistical fluctuations at harder scale, jet triggers based on information from the calorimeters with p_T thresholds at 20

and 40 GeV were also used to collect data. A beam-halo background filter is applied to the triggered events [22]. Event selection further requires exactly one primary vertex, reconstructed in the tracking fit with more than four degrees of freedom, well centered with respect to the z-position of the beam-spot within ± 10 cm.

For each selected event the reconstructed track collection needs to be cleaned up from undesired tracks, namely secondaries and background (e.g. combinatorial background and beam halo associated tracks). Fake tracks coming from mis-reconstruction are removed by requiring tracks to pass the *highPurity* [22] selection, which introduce criterion based on the minimum fraction of consecutive hits depending on the pseudorapidity region. Secondary decays are removed by requiring that the impact parameter significance $d_0/\sigma(d_0)$ and the significance of z separation between the track and primary vertex $d_z/\sigma(d_z)$ each to be less than 3. In order to remove tracks with poor momentum measurement, we require the relative uncertainty of the momentum measurement $\sigma(p_T)/p_T$ to be less than 5%. Average reconstruction efficiency for the selected tracks is about 85% which drops to 75% for low p_T tracks and large η while the fake track rate is about 2% but it increases if tracks have small p_T or lie at large η.

The event energy scale and reference direction, for identification of the UE sensitive region, are defined using leading track-jets [23]. The track-jet collections used in this study consist of jets that are reconstructed from charged tracks with $p_T > 0.5$ GeV and $|\eta| < 2.5$ using the SisCone [24] algorithm with distance parameter of 0.5 for compatibility with previous results [4]. A comparison of the UE activity at generator between SisCone and Anti-k_T [25] algorithms was performed and they only differ by a few percents at low leading jet p_T. From all reconstructed track-jets with $|\eta| < 2$ and $p_T > 1.0$ GeV, the leading p_T one is selected as reference. Events without such a jet are not considered in the analysis. Jets are reconstructed with a matching efficiency of 80% at the lowest p_T^{jet} and up to 95% for $p_T^{\text{jet}} > 20$ GeV. The trigger conditions are matched to keep their efficiency as uniform as possible and close to 100%. For $1 < p_T^{\text{jet}} < 25$ GeV, $25 < p_T^{\text{jet}} < 50$ GeV and $p_T^{\text{jet}} > 50$ GeV, we use respectively the minimum bias and the two jet triggered samples, corresponding to about 11M, 50K and 23K finally selected events.

3.3 Corrections and systematic uncertainties

The UE observables described in section 3.1 are reconstructed from all selected tracks with $p_T > 0.5$ GeV and $|\eta| < 2$ in the *transverse* region to the leading track-jet. These measured observables are corrected for detector effects and selections efficiencies to reflect the activity from all primary charged particles in the same kinematic domain. An iterative unfolding technique [26] is used based on the 4-dimensional response matrices of the multiplicities or scalar-p_{T} sums as a function and p_T^{jet} based on simulated events from the PYTHIA6 Z2 tune. An unfolding of the PYTHIA8 4C reconstructed events based on response matrices obtained from Z2 is used to estimate the systematic uncertainties related to the correction procedure. These vary between 1% and 4% depending on the observables and p_T^{jet}.

Several other sources of systematic uncertainties may affect the results. These include the implementation of the simulation of track and vertex selection criteria, tracker alignment and material content, background contamination, trigger conditions and pile-up contamination. The uncertainty in the simulation of track selection has been evaluated by applying various sets of criteria and comparing their effects to the data and to simulated events. The impact parameter significance cuts are varied by one unit around the nominal cut resulting in an effect on the densities of 2 to 4%. It has also been checked that replacing the *highPurity* selection by a simple cut of $N_{layers} \geq 4$ and $N_{pixellayers} \geq 2$ for silicon and pixel detector layers respectively has an effect of only 0.2%. Varying the track fake rate by 50% affects the densities by 0.4 to 0.5%.

Table 1: Summary of the systematic uncertainties (in percentage) due to various sources.

Source	Systematic (%)
Correction procedure	1 – 4
Impact parameter sig.	2 – 4
Fake	0.4 – 0.5
Track selection	0.2
Material density	1.0
Dead channels	0.1
Tracker alignment	0.2 – 0.3
Beamspot	0.2
Total	2.5–5.8

The description in the simulation of inactive tracker material has been found to be adequate within 5% and increasing the material densities by 5% in the simulation induces a change of the observables by 1%. The effects of tracker misalignment and beamspot position precision and dead channels are all found to change the results by 0.1 to 0.3%. The effect of varying the trigger and vertex efficiencies within their uncertainties as well as the effect of pile-up have all been found to lead to a negligible effect.

Systematic uncertainties are largely independent of one another, but they are correlated among data points in each observable. They are added in quadrature to statistical uncertainties and represented in all figures. Table 1 shows a summary of the quoted systematic uncertainties.

4 Results

The unfolding of the charged particle particle density and Σp_T density was performed. In Fig. 1, the particle (a) and Σp_T (b) densities in the *transverse* region as a function of transverse momentum of a leading charged particle jet are shown. Both measured distributions rise fast for $p_T^{\text{jet}} \lesssim 8$ GeV, attributed mainly to the increase of MPI activity [10], followed by a plateau-like region with nearly constant average number of charged particles and a slow increase of $\sum p_T$ indicating an increase of the amount of energy delivered per particle as the scale of the interaction increases. The data are compared with various MC predictions. In general, all PYTHIA6 and PYTHIA8 tunes predict the distinctive change of the amount of activity as a function of the leading jet p_T, except for PYTHIA8 4C which undershoots the data for $p_T^{\text{jet}} > 5$ GeV. The latest PYTHIA6 (PYTHIA8) tune CUETP6S1 (CUETP8S1) improves the description of the data in comparison with previous tune Z2* (4C). The best description of data in the *transverse* region is achieved by PYTHIA8 CUETP8S1.

In Figs. 2 and 3 particle (a) and Σp_T (b) densities as a function of transverse momentum of a leading charged-particle jet in the *transverse* region with maximum activity (*transMAX*) and with minimum activity (*transMIN*) are shown. In the *transMIN* region, the amount of activity is roughly two times smaller compared to *transMAX*. The shape is also quite different in both categories, at high-p_T the distributions show a slow rise in *transMAX*, while in *transMIN* the plateau-like region is more pronounced. The best description of the data is achieved by PYTHIA8 CUETP8S1 and the description of the data is slightly worse in the *transMIN* than in *transMAX* region.

The difference between *transMAX* and *transMIN* regions (*transDIF*) is presented in Fig. 4. As

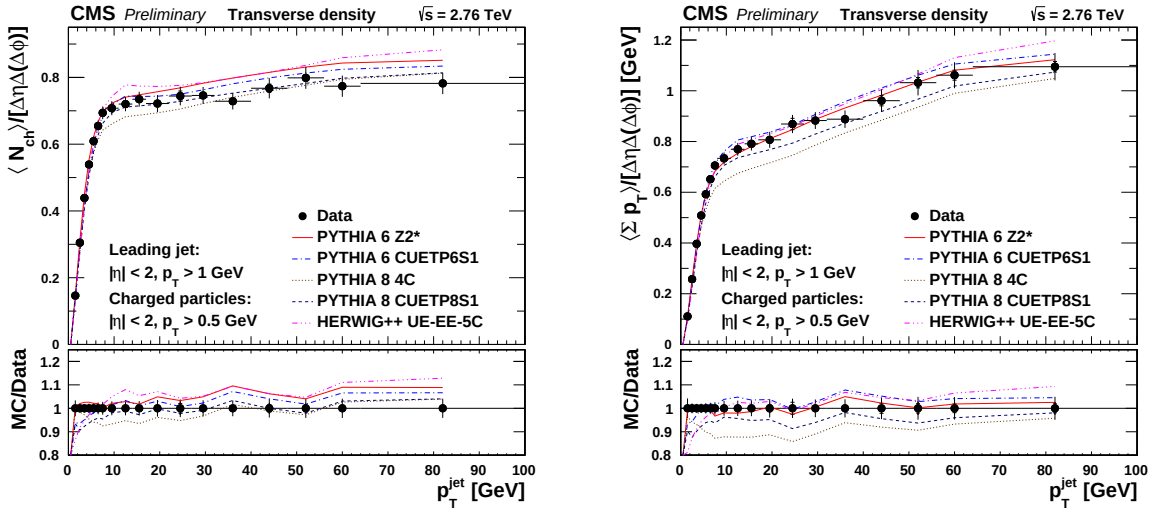

(a) (b)

Figure 1: Measured particle density (a) and Σp_T density (b) in the *transverse* region ($|\eta| < 2, 60^\circ < |\Delta\varphi| < 120^\circ$), as a function leading charged-particle jet p_T. The data are compared to various Monte Carlo predictions. The ratios of MC predictions to the measurements are shown on the bottom of the figure. The inner errors correspond to the statistical uncertainties and the outer errors represent the statistical and systematic uncertainties added in quadrature.

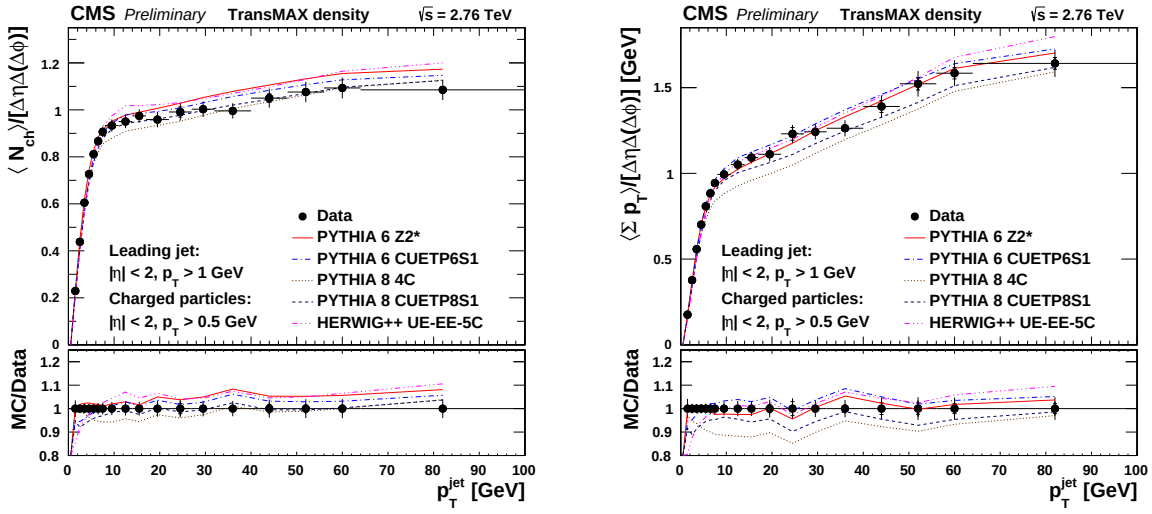

(a) (b)

Figure 2: Measured particle density (a) and Σp_T density (b) in the *transMAX* region with maximum activity within $60^\circ < |\Delta\varphi| < 120^\circ$, as a function leading charged-particle jet p_T. The data are compared to various Monte Carlo predictions. The ratios of MC predictions to the measurements are shown on the bottom of the figure. The inner errors correspond to the statistical uncertainties and the outer errors represent the statistical and systematic uncertainties added in quadrature.

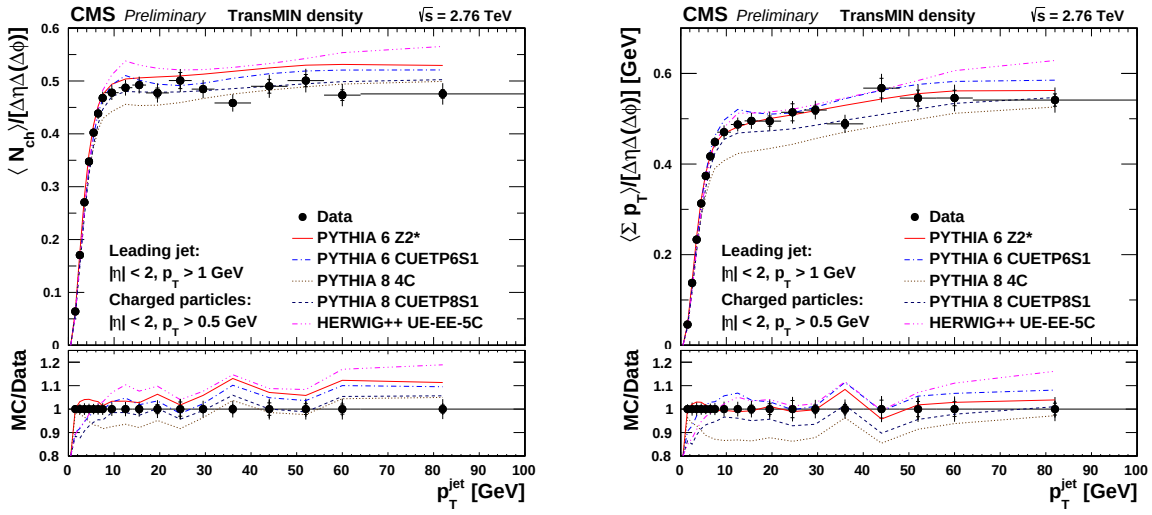

(a) (b)

Figure 3: Measured particle density (a) and Σp_T density (b) in the *transMIN* region with minimum activity within $60^\circ < |\Delta\varphi| < 120^\circ$, as a function of leading charged-particle jet p_T. The data are compared to various Monte Carlo predictions. The ratios of MC predictions to the measurements are shown on the bottom of the figure. The inner errors correspond to the statistical uncertainties and the outer errors represent the statistical and systematic uncertainties added in quadrature.

discussed earlier this distribution is expected to be sensitive to the final- and initial-state radiations. Both particle (Fig. 4 (a)) and Σp_T density (Fig. 4 (b)) show a rise with p_T^{jet} and the plateau-like region at about $p_T^{\text{jet}} \simeq 8$ GeV as seen in the previous plots is not well pronounced here. This is consistent with the *transDIF* activity being sensitive to the initial- and final-state radiation. The same trend is observed in [3]. Different tunes of PYTHIA6 and PYTHIA8 provide a reasonable description of the data.

From Figs. 2 , 3 and 4 one can conclude that the activity from MPI and beam-beam remnant is almost independent on the hard scale for $p_T^{\text{jet}} \gtrsim 8$ GeV, while activity from initial- and final-state radiations increases with p_T^{jet}.

The center-of-mass energy dependence of the activity in the *transverse* region is presented in Fig. 5 as a function of the leading charged-particle jet for $\sqrt{s} = 0.9$, 2.76 and 7 TeV. A strong growth with increasing center-of-mass energy of the activity in the *transverse* region is observed for the same value of the leading charged-particle jet p_T. PYTHIA8 CUETP8S1 predicts the center-of-mass energy dependence of the activity well.

5 Summary

This paper presents a study of the production of charged particles with $p_T > 0.5$ GeV and $|\eta| < 2$ at the LHC with the CMS detector in proton-proton collisions at $\sqrt{s}$ = 2.76 TeV. Events were selected according to the hard scale of the process, provided by the transverse momentum of the leading charged-particle jet, which extends up to 100 GeV. The particle and Σp_T densities are studied in the *transverse* region, defined by the difference in azimuthal angle between the leading track-jet and charged particle directions, $60^\circ < |\Delta\phi| < 120^\circ$, which is appropriate

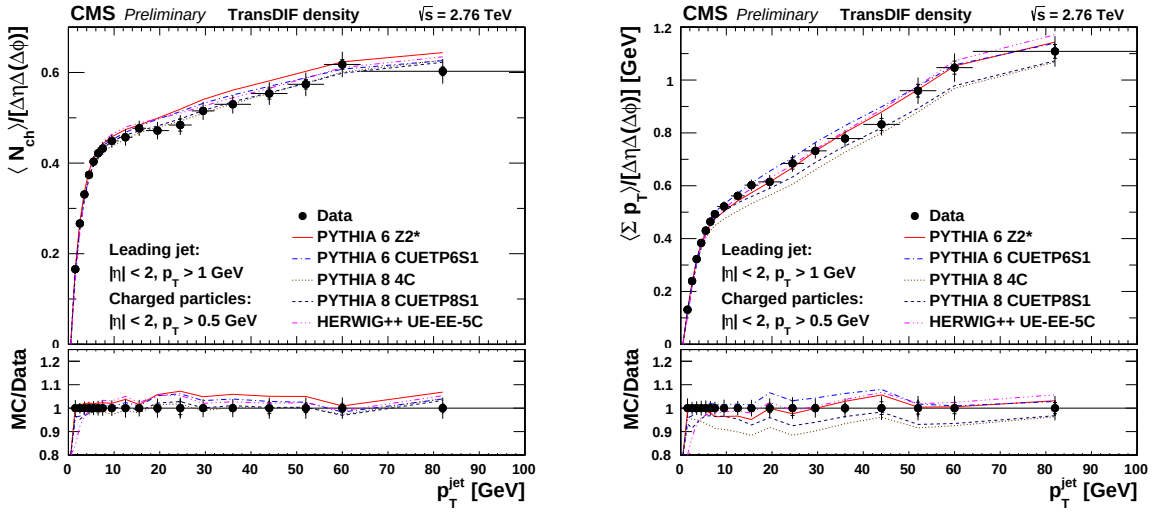

(a) (b)

Figure 4: Measured difference of the activity in the *transDIF* region, ($|\eta| < 2, 60^\circ < |\Delta\varphi| < 120^\circ$), between maximum and minimum activity regions for particle density (a) and Σp_T density (b) as a function leading charged-particle jet p_T. The data are compared to various Monte Carlo predictions. The ratios of MC predictions to the measurements are shown on the bottom of the figure. The inner errors correspond to the statistical uncertainties and the outer errors represent the statistical and systematic uncertainties added in quadrature.

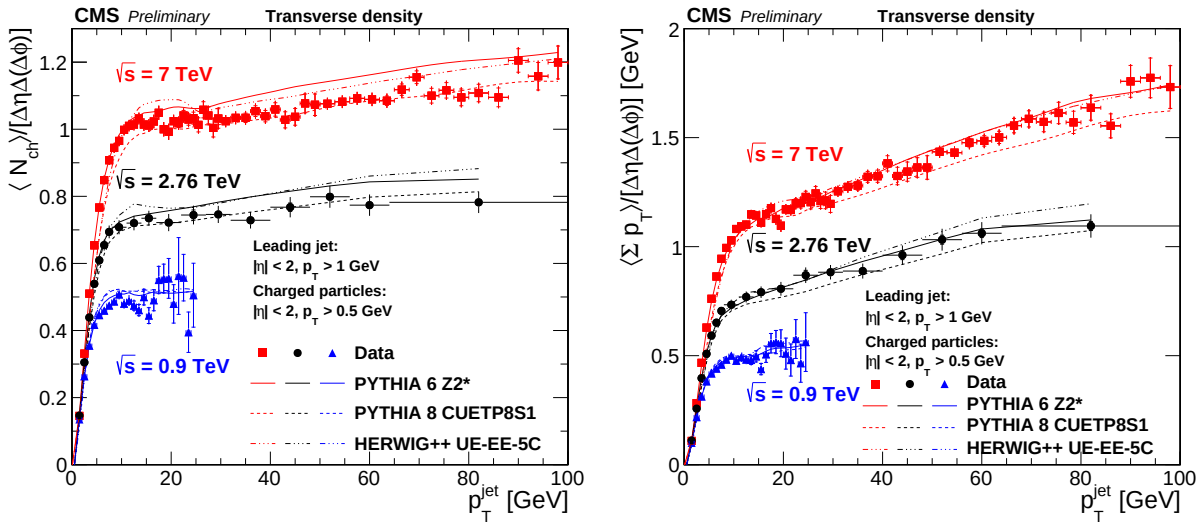

(a) (b)

Figure 5: Comparison of UE activity at $\sqrt{s} = 0.9$, 2.76 and 7 TeV for for particle density (a) and Σp_T density (b) as a function of leading charged-particle jet p_T.

for the study of the underlying event. All distributions were fully corrected for detector effects. The observables have been further subdivided into *transMAX* and *transMIN* regions on an event-by-event basis depending on which side of the event had more activity: this subdivision provides additional discriminating power between the component processes of the UE. In addition, the difference of the hadronic activity in the *transverse* region between maximum and minimum activity regions is also measured. This distribution is expected to be sensitive to the final- and initial-state radiations.

A steep rise of the underlying event activity in the *transverse* region is seen with increasing leading jet p_T. This fast rise is followed by a "saturation" region above $\sim$ 8 GeV, with nearly constant multiplicity and small Σp_T density increase. The events at the high end of the distributions indicate the presence of a hard component in the *transverse* region. Such a distinct change of the amount of activity depending on the transverse momentum of the leading charged-particle jet is clearly seen for all the observables presented in the paper although for *transMAX* and *transDIF* regions the distributions show a rise with p_T^{jet} also at high-p_T tail, corroborating the hypothesis of an increasing contribution from radiation.

The results are compared to recent tunes of PYTHIA and Herwig++ Monte Carlo event generators. PYTHIA6, PYTHIA8 and Herwig++ tunes describe the data within $5-10\%$, except for PYTHIA8 4C which undershoots the data for $p_T^{\text{jet}} > 5$ GeV. In general, the description of the data by the various predictions gets better in *transDIF* region.

By comparing data taken at $\sqrt{s} = 0.9$, 2.76 and 7 TeV, a strong growth with increasing center-of-mass energy of the hadronic activity in the *transverse* region is also observed for the same value of the leading charged-particle jet p_T due to the higher MPI multiplicity, as discussed in section 2. PYTHIA8 CUETP8S1 predicts the center-of-mass energy dependence of the hadronic activity in a way that is very similar to data.

These data provide a detailed measurement of the pp underlying event in QCD jet events, with momentum sums and charged-particle multiplicities. The observables measured in the *transverse*/*transMAX*/*transMIN* regions enable more specific MC model comparisons than possible with preceding available data. These measurements are hence expected to play a significant role in the future development and tuning of MC models of the underlying event.

References

[1] CDF Collaboration, "Charged jet evolution and the underlying event in proton-antiproton collisions at 1.8 TeV", *Phys. Rev. D* **65** (2002) 092002, doi:10.1103/PhysRevD.65.092002.

[2] CDF Collaboration, "Underlying event in hard interactions at the Fermilab Tevatron $\overline{p}p$ collider", *Phys. Rev. D* **70** (2004) 072002, doi:10.1103/PhysRevD.70.072002.

[3] CDF Collaboration, "Studying the underlying event in Drell-Yan and high transverse momentum jet production at the Tevatron", *Phys. Rev. D* **82** (2010) 034001, doi:10.1103/PhysRevD.82.034001.

[4] CMS Collaboration, "Measurement of the underlying event activity at the LHC with $\sqrt{s} = 7$ TeV and comparison with $\sqrt{s} = 0.9$ TeV", *JHEP* **09** (2011) 109, doi:10.1007/JHEP09(2011)109.

[5] CMS Collaboration, "First measurement of the underlying event activity at the LHC with $\sqrt{s} = 0.9$ TeV", *Eur. Phys. J. C* **70** (2010) 555, doi:10.1140/epjc/s10052-010-1453-9.

[6] ALICE Collaboration, "Underlying Event measurements in pp collisions at $\sqrt{s} = 0.9$ and 7 TeV with the ALICE experiment at the LHC", *JHEP* **07** (2012) 116, doi:10.1007/JHEP07(2012)116.

[7] ATLAS Collaboration, "Measurement of underlying event characteristics using charged particles in pp collisions at $\sqrt{s} = 900$ GeV and 7 TeV with the ATLAS detector", *Phys. Rev. D* **83** (2011) 112001, doi:10.1103/PhysRevD.83.112001.

[8] CMS Collaboration, "Measurement of the underlying event in the Drell-Yan process in proton−proton collisions at $\sqrt{s} = 7$ TeV", *Eur. Phys. J. C* **72** (2012) 2080, doi:10.1140/epjc/s10052-012-2080-4.

[9] T. Sjöstrand and M. V. Zijl, "Multiple parton-parton interactions in an impact parameter picture", *Physics Letters B* **188** (1987) 149, doi:http://dx.doi.org/10.1016/0370-2693(87)90722-2.

[10] L. Frankfurt, M. Strikman, and C. Weiss, "Transverse nucleon structure and diagnostics of hard parton-parton processes at LHC", *Phys. Rev. D* **83** (2011) 054012, doi:10.1103/PhysRevD.83.054012.

[11] T. Sjöstrand, S. Mrenna, and P. Skands, "PYTHIA 6.4 physics and manual", *JHEP* **05** (2006) 026, doi:10.1088/1126-6708/2006/05/026, arXiv:hep-ph/0603175.

[12] T. Sjöstrand, S. Mrenna, and P. Z. Skands, "A Brief Introduction to PYTHIA 8.1", *Comput.Phys.Commun.* **178** (2008) 852, doi:10.1016/j.cpc.2008.01.036, arXiv:0710.3820.

[13] M. Bähr et al., "Herwig++ physics and manual", *Eur. Phys. J. C* **58** (2008) 639, doi:10.1140/epjc/s10052-008-0798-9.

[14] T. Sjostrand and P. Z. Skands, "Transverse-momentum-ordered showers and interleaved multiple interactions", *Eur. Phys. J. C* **39** (2005) 129, doi:10.1140/epjc/s2004-02084-y, arXiv:hep-ph/0408302.

[15] CMS Collaboration, "Measurement of energy flow at large pseudorapidities in pp collisions at $\sqrt{s} = 0.9$ and 7 TeV", *JHEP* **11** (2011) 148, arXiv:1110.0211.

[16] CMS Collaboration, "Underlying Event Tunes and Double Parton Scattering", CMS Physics Analysis Summary CMS-PAS-GEN-14-001, 2014.

[17] R. Corke and T. Sjöstrand, "Interleaved parton showers and tuning prospects", *JHEP* **03** (2011) 032, doi:10.1007/JHEP03(2011)032, arXiv:1011.1759.

[18] M. H. Seymour and A. Siodmok, "Constraining MPI models using σ_{eff} and recent Tevatron and LHC Underlying Event data", *JHEP* **1310** (2013) 113, doi:10.1007/JHEP10(2013)113, arXiv:1307.5015.

[19] CMS Collaboration, "Description and performance of track and primary-vertex reconstruction with the CMS tracker", arXiv:1405.6569.

[20] CMS Collaboration, "The CMS experiment at the CERN LHC", *JINST* **03** (2008) S08004, doi:10.1088/1748-0221/3/08/S08004.

[21] J. Pumplin, "Hard underlying event correction to inclusive jet cross sections", *Phys. Rev. D* **57** (1998) 5787, doi:10.1103/PhysRevD.57.5787.

[22] CMS Collaboration, "CMS tracking performance results from early LHC operation", *Eur. Phys. J. C* **70** (2010) 1165, doi:10.1140/epjc/s10052-010-1491-3.

[23] CMS Collaboration, "Performance of Jet Reconstruction with Charged Tracks only", CMS Physics Analysis Summary CMS-PAS-JME-08-001, 2008.

[24] G. P. Salam and G. Soyez, "A practical seedless infrared-safe cone jet algorithm", *JHEP* **05** (2007) 086.

[25] M. Cacciari, G. P. Salam, and G. Soyez, "The anti-k_t jet clustering algorithm", *JHEP* **04** (2008) 063, doi:10.1088/1126-6708/2008/04/063, arXiv:0802.1189.

[26] G. D'Agostini, "A multidimensional unfolding method based on Bayes' theorem", *Nuclear Instruments and Methods in Physics Research Section A: Accelerators, Spectrometers, Detectors and Associated Equipment* **362** (1995) 487, doi:http://dx.doi.org/10.1016/0168-9002(95)00274-X.